









Cite this: DOI: 10.1039/d5lf00218d

# A mussel-inspired cold-water fish gelatin adhesive for surface endothelialization

Tobias Hammer, <sup>†a</sup> Asra Abukar,<sup>†b</sup> Annina Stuber, <sup>cd</sup> Nako Nakatsuka, <sup>d</sup>  
Wuchao Wang,<sup>a</sup> René M. Rossi, <sup>a</sup>  
Costanza Giampietro <sup>\*be</sup> and Kongchang Wei <sup>\*af</sup>

The global burden of cardiovascular diseases has been a driving force for a multitude of medical innovations in the biomedical sector, resulting in the creation of various life-saving implants and devices to alleviate patients' suffering. Despite these advancements, many devices remain susceptible to early failure due to complications during integration within the host body. One of the most common causes is the formation of thrombi due to undesired interactions between blood and the artificial surfaces of implanted devices. To address this issue, modern implants are engineered to exhibit surface properties that promote the formation of an endothelial monolayer, often involving surface biochemical functionalization with cell-adhesive coating agents. In this study, we developed a biopolymeric adhesive based on cold-water fish gelatin (cfGel), a non-mammalian cell-adhesive polymer with numerous advantages over its mammalian counterparts. Inspired by the excellent wet adhesion of mussels, cfGel was functionalized with thiourea-catechol (TU-Cat) groups, resulting in the functional biopolymer (cfGel-TU-Cat) capable of stably adhering to surfaces without the need for additional crosslinking. As proof of concept, cfGel-TU-Cat was demonstrated to promote both the adhesion and proliferation of human umbilical vein endothelial cells (HUVECs) and to support the formation of confluent endothelial monolayers, thus demonstrating its potential as a coating agent for cardiovascular devices.

Received 31st July 2025,  
Accepted 25th November 2025

DOI: 10.1039/d5lf00218d

rsc.li/RSCApplInter

## 1. Introduction

Biomedical innovation in cardiovascular care is in acute demand due to the increasing global burden of cardiovascular diseases (CVDs).<sup>1</sup> However, regardless of the effort dedicated to innovation in this field, many affected patients are still suffering from the early failure of these life-saving implements, especially those with blood-contacting surfaces, such as artificial heart valves, vascular stents, vascular grafts, total artificial hearts (TAHs) and ventricular assist devices

(VADs).<sup>2</sup> Thrombus formation, induced by direct contact of artificial surfaces with blood, is commonly the primary cause of failure, which can be triggered by various reasons such as non-specific adsorption of proteins and subsequent platelet adhesion, and inherent surface properties of the used materials (*e.g.* metals).<sup>2</sup> While certain modifications can enhance the hemocompatibility of blood-contacting devices, their patency rate will inevitably suffer a steady decline without the formation of a permanent layer of endothelial cells (ECs), which can act as a barrier between blood and any adjacent surface to prevent thrombosis.<sup>2–4</sup> Native endothelial monolayers are known to be pivotal for maintaining the cardiovascular system due to their important functions ranging from hemostatic balance and modulation of anti-apoptotic pathways to immunogenicity and control over the contractile activity of blood vessels.<sup>5</sup> Therefore, surface endothelialization, a process to establish such endothelial monolayers, has become a major goal in cardiovascular device innovations. For instance, *in vitro* pre-seeding of ECs has shown great promise for this purpose.<sup>6–8</sup> However, as *in vitro* cultivation is involved, it remains a time-consuming and costly procedure, with considerable complexity and regulatory hurdles that limit its practical application, similar to other *in vitro* cardiovascular tissue engineering approaches.<sup>9</sup>

<sup>a</sup> Empa, Swiss Federal Laboratories for Materials Science and Technology, Laboratory for Biomimetic Membranes and Textiles, Lerchenfeldstrasse 5, 9014 St. Gallen, Switzerland. E-mail: kongchang.wei@empa.ch

<sup>b</sup> Department of Mechanical and Process Engineering, ETH Zurich, Zurich 8092, Switzerland

<sup>c</sup> Laboratory of Biosensors and Bioelectronics, ETH, Zürich, Switzerland

<sup>d</sup> Laboratory of Chemical Nanotechnology, EPFL, 1202, Geneva, Switzerland

<sup>e</sup> Empa, Swiss Federal Laboratories for Materials Science and Technology, Laboratory for Experimental Continuum Mechanics, Überlandstrasse 129, 8600 Dübendorf, Switzerland. E-mail: costanza.giampietro@empa.ch

<sup>f</sup> Empa, Swiss Federal Laboratories for Materials Science and Technology, Laboratory for Biointerfaces, Lerchenfeldstrasse 5, 9014 St. Gallen, Switzerland

<sup>†</sup> Equal contribution.

Alternatively, emerging surface engineering technologies have been exploited to promote *in situ* endothelialization of cardiovascular devices after implantation.<sup>10</sup> Both topological and biochemical surface modification have been used either independently or cooperatively to promote surface endothelialization.<sup>11–14</sup> Topographical patterning of surfaces on the micro- and nano-scale can guide the growth of endothelial cells into an elongated and aligned morphology, thus allowing the pre-defining of growth-patterns for ECs akin to native healthy endothelium.<sup>15–17</sup> However, this strategy frequently requires prior biochemical surface functionalization involving the covalent or non-covalent immobilization of cell adhesive biomolecules that can induce specific binding of EC membrane receptors, thus improving cell-attachment and surface endothelialization.<sup>18–22</sup> The coating agents used for these surface modifications mainly include cell-adhesive peptides and proteins, as well as protein-derived biopolymers such as gelatin.<sup>23–25</sup>

Gelatin has found prominent use in the biomedical sector due to its inherent bioactive properties, biocompatibility and degradability, and its status as a material regarded as safe by the United States Food and Drug Administration (FDA).<sup>26</sup> As gelatin is derived from the denaturation of collagen, it retains many of the beneficial characteristics of its parent protein, including an abundance of arginine–glycine–aspartate (RGD)-sequences, while simultaneously being less antigenic than collagen itself.<sup>27,28</sup> Furthermore, gelatin exhibits a diverse array of functional groups available for chemical modifications, thus allowing it to be tailored towards specific applications.<sup>29</sup> While gelatin derived from mammalian tissues (*e.g.* pig skin) constitutes the most widely used variant, alternative sources are desirable due to the growing sociocultural and health-related concerns.<sup>30,31</sup> Among the potential candidates, gelatin extracted from cold-water fish (cfGel) has garnered significant attention due to its low gelling and melting point, economical sourcing as a product from fish waste, reduced risk for disease transmission, and general sociocultural acceptance regarding its consumption and bodily incorporation.<sup>30,32,33</sup> The low gelling and melting point allow cfGel to remain liquid at ambient temperatures, thus greatly simplifying processing and handling of the material without the need for elevated temperatures.<sup>33</sup>

Previously, we developed a biopolymeric hydrogel adhesive from catechol (Cat) modified porcine gelatin capable of forming stable adhesion on wet tissue surfaces, while simultaneously supporting the growth of human umbilical vein endothelial cells (HUVECs).<sup>34</sup> Compared to the commonly used amide linkage between polymer backbones and Cat groups, thiourea (TU) linkage was used to mimic the reducing thiol groups of mussel foot protein-6 (MFP-6) and improve wet adhesion performance of Cat-functionalized hydrogels. Given the aforementioned advantages of cfGel, we herein developed a multifunctional biopolymer from cfGel to promote surface endothelialization. Specifically, to mimic the adhesive properties of MFPs, TU-Cat groups were grafted onto cfGel, giving rise to cfGel-TU-Cat polymers containing

both the intrinsically inherent RGD sequences of cfGel for promoting cell attachment, as well as TU-Cat functionalities for the formation of stable surface coatings (Fig. 1). It is noteworthy that the majority of cfGel polymers that have emerged for biomedical applications exhibit modifications with methacrylate or norbornene functional groups in order to enable photo-initiated crosslinking into hydrogels for direct cell encapsulation or 3D bioprinting.<sup>32,35,36</sup> Herein, the dual-adhesive property to both cells and substrates conferred onto cfGel through the TU-Cat modification offers new potential for biomedical applications of cfGel, especially in cardiovascular device innovations.

## 2. Experimental section

### 2.1 Materials

Gelatin from cold-water fish skin (Sigma-Aldrich, G7041-500G), dopamine hydrochloride (Dopamine-HCl, as a white powder), sodium sulfate anhydrous (Na<sub>2</sub>SO<sub>4</sub>), triethylamine (TEA, ≥99.5%), carbon disulfide (CS<sub>2</sub>, ≥99.9%), hydrogen peroxide solution (H<sub>2</sub>O<sub>2</sub>, containing inhibitor, 30 wt% in H<sub>2</sub>O, ACS reagent), peroxidase from horseradish (HRP, type VI, essentially salt-free, lyophilized powder, ≥250 units per mg of solid), deuterated dimethyl sulfoxide (DMSO-d<sub>6</sub> with 99.96 atom %D), hydrochloric acid (HCl, ACS reagent, 37 wt%), and dimethyl sulfoxide (DMSO, ≥99%) were purchased from Sigma-Aldrich. Tetrahydrofuran (THF, ≥99%) and methanol (≥99%) were purchased from Fisher Chemical. All chemicals were used as received unless specified otherwise. Dry regenerated cellulose (RC) membranes (Spectra/Por 1, 6–8 kDa MWCO) were purchased from Faust (Switzerland).

Porcine gelatin (#104070; Merck Millipore), PBS (#10010-015; Thermo Fisher Scientific), primary human umbilical vein endothelial cells (HUVECs, #C-12203; Promocell, pooled donors), endothelial cell growth medium (C22010; Promocell), BCA Protein Assay kit (#23227; Thermo Fisher Scientific), iBlot™ Transfer stack nitrocellulose (#IB23001; Thermo Fisher Scientific).

Glutaraldehyde (#35440; Sigma-Aldrich), glycine (#G8790; Sigma Aldrich), 4% PFA (#043368.9M; Thermo Fisher Scientific), Triton X-100 (#T8787; Sigma Aldrich), bovine serum albumin (#A6003, Sigma Aldrich), SDS (#11667289001; Sigma Aldrich), glycerol (#G5516; Sigma Aldrich), Tris-HCl (#108319, Sigma Aldrich), 1× PBS from Thermo Fisher.

### 2.2 Methods

**2.2.1 Synthesis of Dopamine-ITC.** 4-(2'-Isothiocyanatoethyl)-1,2-benzenediol (Dopamine-ITC) was synthesized according to a previously reported procedure.<sup>34</sup> Dopamine-HCl (5.0 g, 26.4 mmol) was partially dissolved in tetrahydrofuran (80 mL) under constant stirring before TEA (4.4 mL, 31.6 mmol) was added. Methanol (80 mL) was added to dissolve Dopamine-HCl. Carbon disulfide (CS<sub>2</sub>, 8.0 mL, 131.9 mmol) was added to the mixture and stirred for 30 min at 25 °C under a nitrogen atmosphere. The reaction mixture was cooled with an ice bath before dropwise addition of



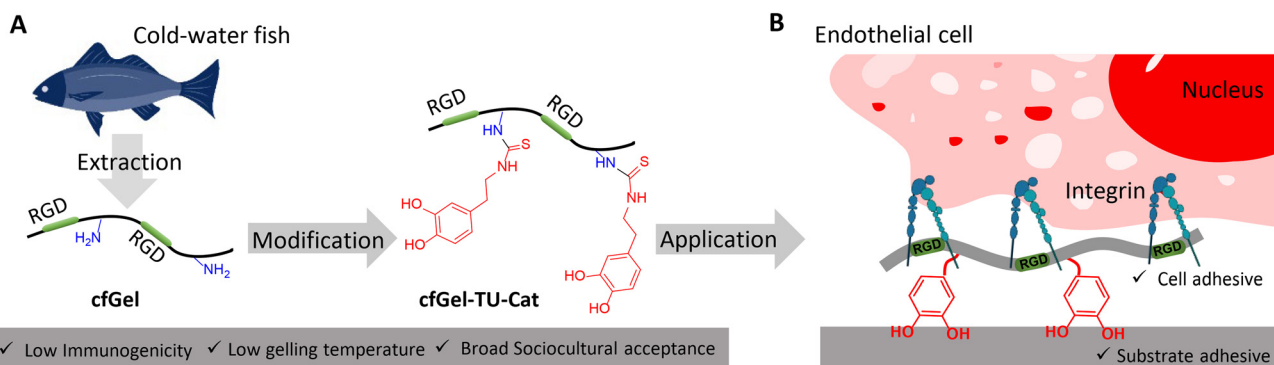


**Fig. 1** (A) Bio-inspired functionalization of cold-water fish gelatin (cfGel). (B) Thiourea-catechol-functionalized polymer (cfGel-TU-Cat) offers both cell adhesive and substrate adhesive properties to promote endothelial cell attachment and surface endothelialization. Created, in part, with <https://BioRender.com>.

H<sub>2</sub>O<sub>2</sub> (6.2 mL, 74.9 mmol). The solution was immediately acidified with HCl (2.64 mL) and then concentrated with a rotary evaporator (at 23 °C, under 300 mbar, and 100 rpm). The resulting mixture was filtered and washed with deionized water (DI water). The filtrate was extracted with ethyl acetate three times (3 × 50 mL). The combined organic layers were dried by Na<sub>2</sub>SO<sub>4</sub> overnight under argon protection. After filtration, the solution was concentrated with a rotary evaporator (at 40 °C, under 200 mbar and 100 rpm) to give the viscous oil-like product, which was used freshly for the synthesis of cfGel-TU-Cat without further purification.

**2.2.2 Synthesis and characterization of cfGel-TU-Cat.** Dopamine functionalized cold-water fish gelatin (cfGel-TU-Cat) was synthesized by conjugating Dopamine-ITC to the primary amine groups of gelatin.<sup>34</sup> Briefly, Dopamine-ITC (5.6 g) was dissolved in a mixture of DI water/DMSO (1:2, 150 mL) at 25 °C. Then cold-water fish gelatin (cfGel, 10 g) was added to the solution under nitrogen atmosphere. The mixture was left stirring for 19 h at 50 °C under nitrogen atmosphere. The resulting solution was purified by dialysis (MWCO 6–8 kDa) against a DI water/DMSO mixture (1:2) for 8 hours (500 mL × 4 times), and then against DI water (4 L) for 3 days (refreshing water 4 times per day) at 25 °C prior to lyophilization to obtain the final product. For <sup>1</sup>H NMR characterization (Bruker AV III HD 400 MHz), cfGel-TU-Cat (70 mg) was dissolved in 0.7 mL deuterium oxide (D<sub>2</sub>O). For UV-vis absorbance measurement (Cary 50 Bio UV-vis spectrophotometer), a cfGel-TU-Cat/H<sub>2</sub>O solution (15 mg mL<sup>-1</sup>) was used.

The thermal gelation behavior of the synthesized polymer was investigated by inversion test. Briefly, porcine gelatin, cfGel, and cfGel-TU-Cat were dissolved in ultrapure water at a concentration of 10 wt% and the gelation behavior of each polymer solution was evaluated after an incubation period of at least 15 min at various temperatures through an inversion test and visual observation. All three polymer solutions were first incubated in a cabinet at 37 °C to reach the solution state, followed by incubation at 25 °C, 15 °C, 10 °C, 7 °C, and 5 °C in a temperature-controlled water bath. An additional incubation was performed in a fridge at 4 °C overnight.

**2.2.3 Quartz crystal microbalance with dissipation monitoring (QCM-D).** The QSense E4 (Biolin Scientific) was used for QCM-D experiments, and silicon dioxide (SiO<sub>2</sub>)-coated crystals with a 5 MHz resonance frequency were employed (QSensor QXS 303 TiAu/SiO<sub>2</sub> purchased from Microvacuum Ltd.). All chips were cleaned following a 2 min sonication cycle in acetone, isopropanol followed by Milli-Q water, and subsequently dried with nitrogen gas. The chips were ozone cleaned for an additional 30 min (UVO cleaner 42-220). All tubing, gaskets and O-rings were cleaned with 2% sodium dodecyl sulfate, Milli-Q water and then dried with nitrogen gas. The QCM-D sensors were then placed into the system and a voltage was applied to excite the piezoelectric material of the sensing crystal at its resonance frequency. The QCM-D temperature was set between 32–33 °C, and liquids were flushed by using syringe injections. A baseline was acquired in 1× PBS. Either 0.015 wt% polymer (cfGel or cfGel-TU-Cat) solution in 1× PBS were flushed over the QCM-D crystals. The buffer was switched back to 1× PBS, to wash away any unbound polymer. The 7th harmonic has been used to demonstrate frequency and dissipation changes over time in all graphs. The mass change ( $\Delta M$ ) was calculated using the Sauerbrey equation, correlating the change in frequency directly to the change in mass:

$$\Delta M = \frac{-C \times \Delta F}{n} \quad (1)$$

where  $C$  represents the mass sensitivity constant, approximated at 17.7 ng cm<sup>-2</sup> Hz<sup>-1</sup> for the crystals used,  $\Delta F$  (Hz) refers to the change in frequency, and  $n$  the harmonic. The Sauerbrey equation was selected to approximate the mass as we consider the QCM chip is coated with a thin film of polymer.<sup>37</sup> Any readouts with artifacts such as drastic base-line jumps, potentially due to the presence of air-bubbles, were disregarded. If a continuous linear drift was observed, the baseline was fit to a linear regression and subtracted from the values as base-line correction. A total of  $n = 4$  recordings were made for each polymer condition, and the average frequency,

dissipation, and mass was calculated after rinsing away any unbound polymer. Mann-Whitney *U*-test statistics were performed due to the small sample size, we cannot assume a particular population distribution, and we applied a directional hypothesis, testing that the cfGel-TU-Cat results in a thicker layer than the cfGel.

**2.2.4 Substrate coating for cell culture.** The porcine-gelatin crosslinking was performed as previously described.<sup>38</sup> Briefly, the samples were incubated for 1 h at 37 °C with 1.5 wt% gelatin (#104070, Merck Millipore), followed by a crosslinking with 2% glutaraldehyde solution for 15 min at room temperature. The glutaraldehyde was then replaced by 70% ethanol. After 1 h at room temperature, two washes with PBS (Thermo Fisher Scientific) followed by overnight incubation with PBS containing 2 mM glycine were performed. Before cell seeding, slides were washed another 2 times with PBS. Alternatively, substrates were coated with gelatin coating (without glutaraldehyde crosslinking) and cfGel-TU-Cat overnight, then excess was removed, and cells were directly seeded onto the substrates.

**2.2.5 Cell culture.** Primary human umbilical vein endothelial cells (HUVECs; Promocell, pooled donors), were grown in endothelial cell growth medium (C22010, Promocell) and were maintained at 37 °C and 5% CO<sub>2</sub>. All reported experiments were performed using cells with less than six passages *in vitro*, unless otherwise specified.

**2.2.6 Adhesion assay.** Adhesion assay procedure was adapted from the general method described by Humphries, M.<sup>39</sup> Briefly, 96-well plates were coated with either crosslinked or non-crosslinked porcine gelatin and cfGel-TU-Cat (12 replicates each) overnight. As a control, cells (6 replicates) were seeded on non-coated wells. Cells were washed, harvested, and counted, and an equal number of cells (10 000 cells per well) were seeded and allowed to adhere for 20 min at 37 °C. After this period, non-adherent cells were gently removed by washing three times with 100 µl of pre-warmed PBS (pH 7.4, Thermo Fisher Scientific) using a multichannel pipette. The pipette tips were positioned along the well wall to minimize mechanical disturbance of adhered cells. Adherent cells were then fixed with 4% paraformaldehyde (PFA) for 15 min at room temperature and stained with DAPI. Cell adhesion was quantified by acquiring 10 fluorescence images per well using an epifluorescence microscope. Results are expressed as cell number relative to the control (uncoated samples).

**2.2.7 Proliferation assay.** The cells were seeded sparsely (5000 cells per well) on pre-coated glass coverslips and cultured for 48 h. Afterwards the cells were fixed with 4% PFA and stained for Ki67 and DAPI to quantify proliferating cells.

**2.2.8 Paracellular permeability assay.** The assay was carried out as previously reported.<sup>40</sup> Briefly, endothelial monolayers were cultured on biotin-conjugated 1.5 wt% gelatin. At selected time points (3 days after seeding), Oregon Green 488-conjugated avidin (Thermo Fisher Scientific) was added to the culture medium at a final concentration of 25

µg ml<sup>-1</sup> for 3 minutes. The medium was then removed, and the cells were fixed with 37 °C warm 4% paraformaldehyde for 15 minutes. Residual unbound avidin was removed by washing samples with PBS after fixation. Immunofluorescence for VE-cadherin was performed to identify junctional discontinuities.

**2.2.9 Immunofluorescence.** At selected time points, cells were fixed with 4% paraformaldehyde in PBS, permeabilized for 10 min with PBS 0.5% Triton X-100 and incubated for 1 h at room temperature in a blocking solution of PBS with 5% BSA. Subsequently, samples were incubated with primary antibodies diluted in blocking buffer overnight at 4 °C. After washing with PBS, a secondary antibody incubation for 1 h at room temperature was performed. DAPI was used to counterstain nuclei.

**2.2.10 Statistical analysis.** The Shapiro-Wilk test was used to test the normality of the data. For normally distributed data, ANOVA test was performed. The Kruskal-Wallis-test was used for non-normally distributed data. A significance level of 0.05 was used for all tests. Bar plots depict the mean values with error bars for the standard error of the mean SEM. In all box plots the population means are reported as a horizontal line inside the boxplot, the population medians are reported as a small square inside the box plot. The total number of events counted is reported in the figure caption. The number of independent experiments is indicated as *n* and the number of total cells/fields of view is shown as *n'* (\**p* < 0.05, \*\**p* < 0.01, \*\*\**p* < 0.001).

**2.2.11 Image acquisition.** Confocal microscopy was performed at room temperature using an automated Nikon-Ti spinning disk confocal microscope (Nikon) equipped with an Andor DU-888 camera (Oxford Instruments) and a pE100 LED illumination system (CoolLED Ltd.) with violet (405 nm laser diode), blue (488 nm; argon), yellow (561 nm; solid state) and red (633 nm; HeNe) excitation laser lines. Only adjustments of brightness and contrast were used in the preparation of the figures. For comparison purposes, different sample images of the same antigen were acquired under constant acquisition settings. Image acquisition was performed using a 63×/1.4 NA and 40× oil immersion objective (HCX PL APO 63× Lbd BL, Leica). Fluorescent Z-stacks of the signals emitted were acquired selecting the optical filters based on the respective emission. ImageJ version 1.33 was used for data analysis.

**2.2.12 Image analysis.** The fraction of area per field of view stained with biotin-avidin was measured using ImageJ (National Institute of Health). The “measure” option was used to obtain the total area of the field of view. The “automatic threshold” tool and the “measure” option were used to determine the area covered by the biotin-avidin signal. Finally, the fraction of biotin-avidin leakage was obtained by dividing the area covered by the biotin-avidin signal with the total area of the field of view.

**2.2.13 Western blotting.** Western blot analysis was performed according to standard protocols. Cells were lysed in boiling Laemmli sample buffer [2% SDS, 20% glycerol,





and 125 mM Tris-HCl (pH 6.8)], and the protein concentration was determined using a BCA Protein Assay kit (Thermo Fisher Scientific). Equal amounts of proteins were loaded on a gel, separated by SDS-PAGE and transferred to a nitrocellulose membrane (Thermo Fisher Scientific). After blocking, incubation with primary antibodies, and horseradish peroxidase-linked secondary antibodies, specific bindings were detected using a chemiluminescence system (Thermo Fisher Scientific). The bands were quantified using an optic densitometry software (Image Lab 6.0.1, Biorad) and normalized to the levels of an appropriate housekeeping protein.

### 3. Results and discussion

#### 3.1 Synthesis and characterization

The functional polymer cfGel-TU-Cat was synthesized with the method described in the Experimental section 2.2.2, which was adapted from a previous report for porcine gelatin polymers (Fig. 2A).<sup>34</sup> Considering the content of lysine (the

origin of  $\epsilon$ -amino groups for TU-Cat modification) in fish gelatin polymers ( $\sim 3$  mol% of total amino acid residuals, *i.e.*  $\sim 270$   $\mu\text{mol}$  per g polymer), we decided to use 5.6 g Dopamine-ITC for the modification of 10 g cfGel polymer, ensuring a substantially excessive amount of Dopamine-ITC (2.56 mmol for each gram of gelatin) for introducing as many TU-Cat groups as possible to cfGel polymer.<sup>30</sup> Successful functionalization of cfGel was evidenced by the characteristic UV-vis absorbance of catechol groups at 280 nm (Fig. 2B). Catechol content of the functional polymer cfGel-TU-Cat was estimated by  $^1\text{H}$  NMR analysis. The aromatic proton signal of gelatin (*a* and *a'*) observed around  $\sim 7.3$  ppm is primarily attributed to phenylalanine (Phe) residues (Fig. 2C and D), which constitute approximately 1.2–1.6% of the total amino acid content in cfGel.<sup>30</sup> The integration values of Phe signals were normalized (*i.e.*  $I_a = I_{a'} = 100$ ) to assess relative changes in the other aromatic peaks ( $\sim 6.9$  ppm) due to the addition of catechol groups. Due to the overlap of tyrosine (Tyr) and Cat peaks, the increased signal integration value at  $\sim 6.9$  ppm ( $\Delta I = I_{b'} - I_b$ ) was attributed to the catechol groups. Therefore,

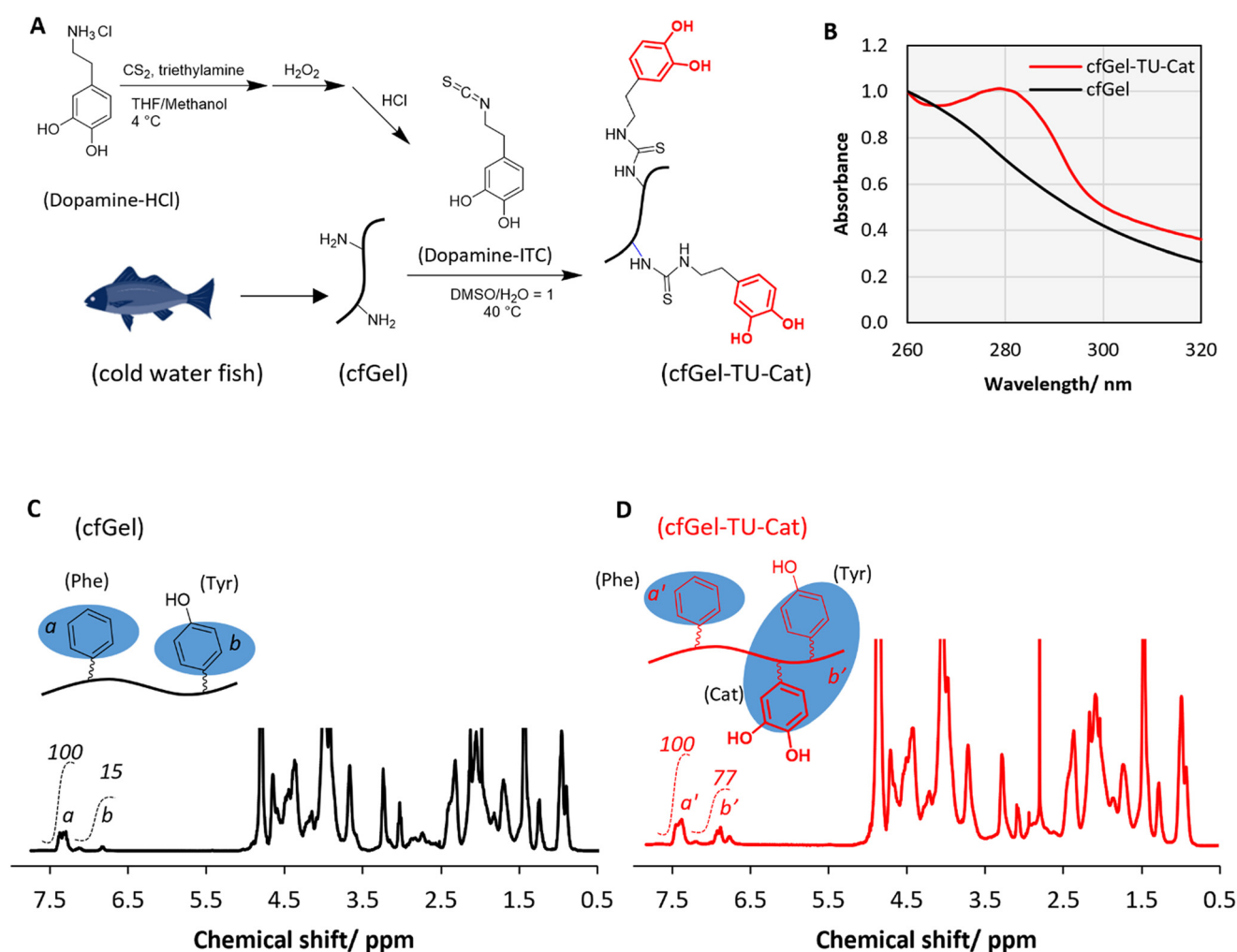


Fig. 2 (A) Chemical synthesis of cfGel-TU-Cat polymers. Created, in part, with <https://BioRender.com>. (B) UV-vis spectra of cfGel and cfGel-TU-Cat polymers. (C)  $^1\text{H}$  NMR analysis of cfGel polymer. (D)  $^1\text{H}$  NMR analysis of cfGel-TU-Cat polymer.



the catechol content can be estimated to be  $X$  times that of Tyr residuals, according to eqn (2):

$$X = \frac{\Delta I}{N_{\text{Cat}}} \times \frac{N_{\text{Tyr}}}{I_b} \quad (2)$$

where  $N_{\text{Cat}}$  and  $N_{\text{Tyr}}$  represent the number of aromatic protons per catechol or tyrosine group, respectively. With  $N_{\text{Cat}} = 3$ ,  $N_{\text{Tyr}} = 4$ ,  $\Delta I = I_b - I_b = (77-15) = 62$ , and  $I_b = 15$ ,  $X$  was calculated to be  $X = 5.5$ . The average amount of Tyr residuals is estimated to be around 0.3–0.4% of the total amino acid content in cfGel.<sup>30</sup> Therefore, the content of catechol functional groups was approximately 1.7–2.2% of the total amino acid content. By using  $110 \text{ g mol}^{-1}$  as the average molecular weight per amino acid residue, this content corresponds to 155–200  $\mu\text{mol}$  catechol groups per gram of polymer.

### 3.2 Substrate adhesion

To verify the substrate adhesion promoted by TU-Cat functional groups, we compared polymer attachment onto glass substrates between unmodified cfGel and cfGel-TU-Cat by using a quartz crystal microbalance with dissipation monitoring (QCM-D). Owing to the high sensitivity of QCM-D to detect even small alterations in mass on its sensor-surface, the deposition and adhesion of the respective polymers could be readily observed.<sup>41</sup> This is especially relevant given that the surface coatings constitute a thin layer of polymer chains, making it challenging to reliably distinguish adhesion differences between two similar polymers with other contemporary methods. Each signal spike corresponds to an instance of solution injection, whereas a change in injection solution is indicated by the arrows (Fig. 3A). Upon polymer solution injections, mass assembly on the chip surface was observed, indicating a deposition of polymer on the sensor-surface (Fig. 3A). After flushing with PBS for  $\sim 100$  min to remove any non-adherent polymer, the mass of the remaining polymer ( $\Delta M$ ) was quantified (Fig. 3B) based on a change in frequency ( $\Delta F$ , Fig. S1) using the Sauerbrey equation (Experimental section 2.2.3).<sup>37</sup> Compared to the average  $\Delta M$  of  $430.18 \pm 166.68 \text{ ng cm}^{-2}$  observed for unmodified cfGel

polymer, cfGel-TU-Cat deposition resulted in a statistically significant ( $p = 0.029$ ) 1.7-fold increase of  $\Delta M$  ( $714.31 \pm 135.04 \text{ ng cm}^{-2}$ ), indicating the substrate-adhesive properties facilitated by the TU-Cat modification. On one hand, this result aligns with the well-established principles of catechol-based adhesion chemistry that allows for the formation of both covalent and non-covalent bonding to various inorganic surfaces even in wet environments.<sup>42</sup> In the case of  $\text{SiO}_2$ , adhesion is mediated through hydrogen bonding owing to the presence of two neighboring hydroxy groups.<sup>42</sup> On the other hand, instead of amide groups used commonly to conjugate catechols to biopolymer chains,<sup>43</sup> the thiourea (TU) groups were reported to be an effective biomimetic of mussel foot protein 6 (Mfp-6), thus preserving the adhesion property *via* a redox-modulated rescue of quinones back to catechols.<sup>34,44,45</sup> Moreover, no significant difference was observed from dissipation changes ( $\Delta D$ , Fig. S1), which indicates a comparable viscoelastic behavior of both polymer layers deposited on the sensors. This finding further implies that the physical properties of gelatin polymer chains were not noticeably altered by TU-Cat modification.

### 3.3 Cell adhesion and proliferation

Gelatin, as a hydrolytic product of collagen, has been a major coating material for *in vitro* culture of cells on various substrates. Comparing the thermal gelation behavior of cfGel-TU-Cat to unmodified cfGel and porcine gelatin revealed that porcine gelatin only remained in solution state at  $37^\circ\text{C}$  but formed gels at and below  $25^\circ\text{C}$  (Fig. S2). In contrast, both cfGel and cfGel-TU-Cat solutions remained fully or partially in solution state at and above  $5^\circ\text{C}$ . Only a prolonged incubation period at  $4^\circ\text{C}$  resulted in the complete gelation of the fish gelatin-based polymer solutions. Consequently, the low gelling temperature enables cfGel-TU-Cat to remain in a solution state at room temperature, which greatly improves the ease of handling and processing of the material. This feature, along with its improved substrate adhesive properties and lower risk of disease transmission, make cfGel-TU-Cat a particularly suitable alternative to mammalian gelatin for cardiovascular devices, where

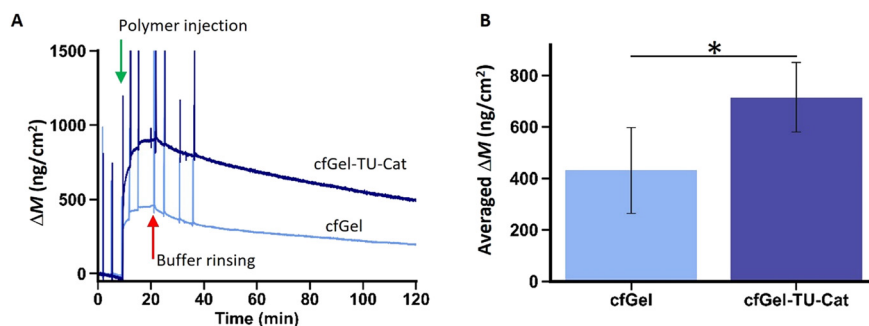


**Fig. 3** Quartz crystal microbalance with dissipation measurements of polymer coatings on  $\text{SiO}_2$  substrates (7th harmonic depicted). (A) Change in mass deposited on sensor surfaces upon polymer injection (green arrow) and buffer rinsing (red arrow). (B) Averaged mass change ( $\Delta M$ ) from  $n = 4$  measurements for the cfGel and cfGel-TU-Cat polymers on the sensor surfaces ( $*p < 0.05$ , Mann-Whitney  $U$  statistic test).



promoted adhesion and growth of endothelial cells are crucial.

As proof of concept, HUVECs were seeded on glass slides coated with different polymers, namely glutaraldehyde (GTA)-crosslinked porcine gelatin (Xlinked PorGel), non-crosslinked porcine gelatin (PorGel) and cfGel-TU-Cat, respectively. As mammalian gelatin is commonly used with or without crosslinking for improving endothelial cell-substrate adhesion, both Xlinked PorGel and PorGel were used as benchmarks for cfGel-TU-Cat.<sup>25,46,47</sup> This comparison aimed to evaluate the potential of cfGel-TU-Cat as an alternative material for promoting endothelial cell-substrate adhesion and facilitating subsequent endothelialization. HUVECs for these evaluations were expanded beforehand for a week in culture flasks coated with either PorGel or cfGel-TU-Cat (Fig. S3).

First, HUVECs were expanded in PorGel-coated flasks. After harvesting, the cells were incubated for 20 minutes on glass substrates coated with different polymers before assessing cell adhesion. No significant difference in cell adhesion (average relative ratio:  $\sim 0.6$ – $0.8$ ) was observed on the three substrates (Fig. 4A and B). This indicates the potential of cfGel-TU-Cat in replacing mammalian gelatin polymers for endothelial cell culture. Furthermore, due to the inherent substrate-adhesive properties of cfGel-TU-Cat, the additional use of any potentially cytotoxic crosslinking agents or methods can be avoided without affecting substrate coating-efficiency.

Subsequently, we performed the same adhesion test with HUVECs expanded in flasks coated with cfGel-TU-Cat (Fig. S4A and B). Cell adhesion on different polymer-coated surfaces was found to have improved (average relative ratio  $\sim 1$ – $1.5$ ), compared to the abovementioned adhesion of cells expanded in PorGel-coated flasks (average relative ratio:  $\sim 0.6$ – $0.8$ ). This indicates that cfGel-TU-Cat may induce a higher pro-adhesive phenotype during cell expansion. Interestingly, when seeded post-expansion, these primed cells showed the highest adhesion on PorGel-coated substrates, suggesting a synergistic interaction between cell-intrinsic changes and surface properties. In contrast, cells expanded on PorGel-coated substrates exhibited consistently lower adhesion, showing no preference among the different substrates (Fig. 4A and B). These findings highlight the dynamic interplay between pre-conditioning environments and subsequent cell adhesion behavior, underscoring the importance of substrate history in adhesion assays. Moreover, cell proliferation was quantified by Ki67 staining. The fraction of Ki67-positive cells revealed comparable rates of cell proliferation on the different substrates (Fig. 4C and D), regardless of the type of polymer-coating that has been previously used for cell expansion (Fig. S4C and D).

### 3.4 EC monolayer permeability

We further evaluated the endothelial functions from HUVEC monolayers established on different substrates by

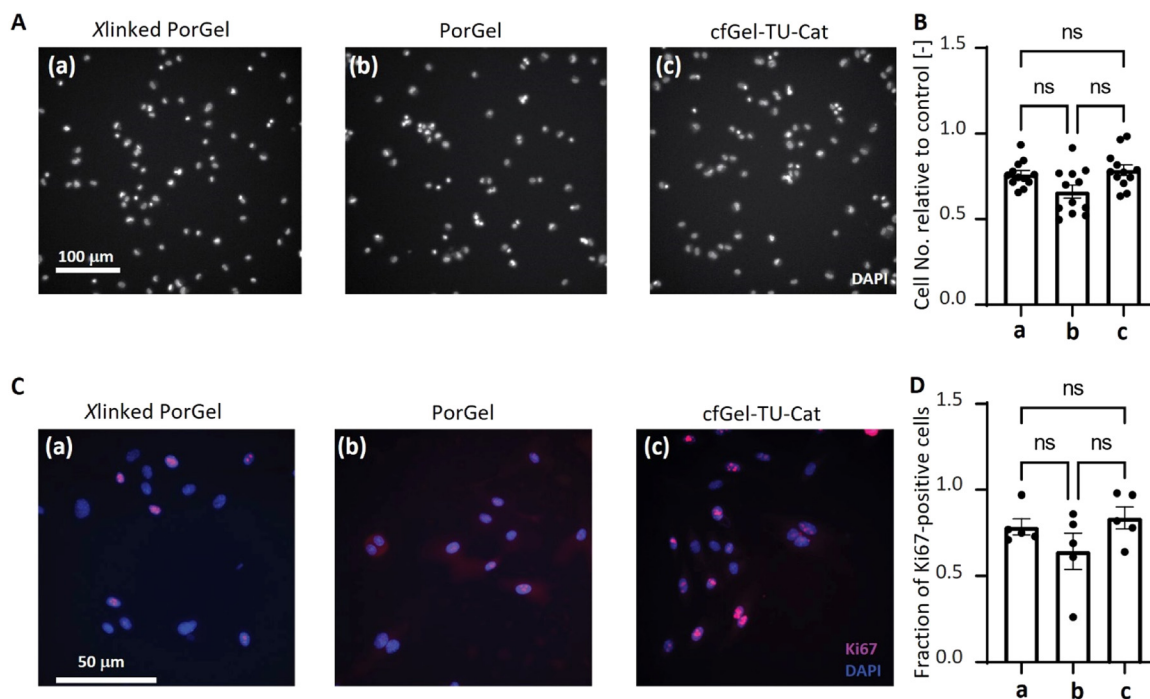


**Fig. 4** Cell adhesion and proliferation assays of HUVECs (expanded in PorGel-coated flasks). (A) Cells adhered on glass substrates with different coatings (a) Xlinked PorGel, (b) PorGel, and (c) cfGel-TU-Cat were visualized by DAPI staining of cell nuclei. (B) Relative changes of adhered cell numbers on different substrates coated with (a) Xlinked PorGel, (b) PorGel, and (c) cfGel-TU-Cat,  $n = 3$ . (C) Cells were visualized with Ki67 and DAPI staining for proliferation assay. (D) Fraction of Ki67-positive cells on different substrates coated with (a) Xlinked PorGel, (b) PorGel, and (c) cfGel-TU-Cat,  $n = 3$ .



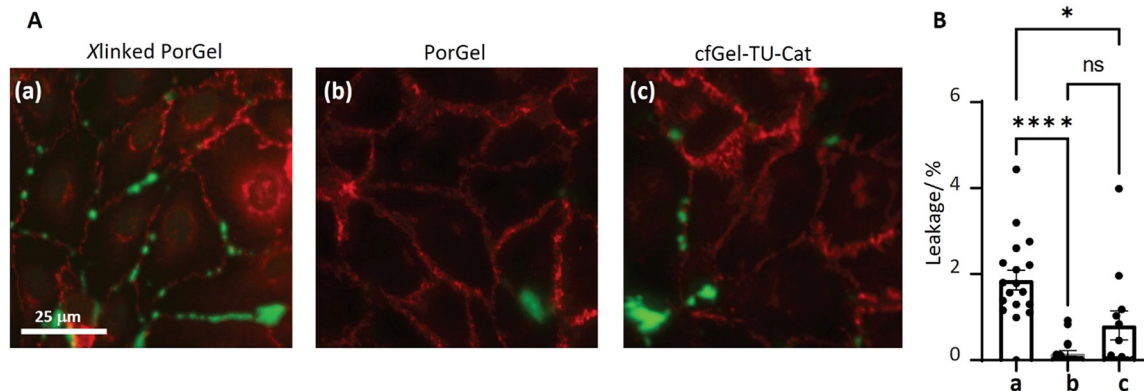


**Fig. 5** Effects of different substrate coatings on the permeability of monolayer cells developed from HUVECs expanded in PorGel-coated flasks. (A) VE-cadherin (red) and biotin-avidin (green) immunofluorescent staining of cells grown on different substrates coated with (a) Xlinked PorGel, (b) PorGel, and (c) cfGel-TU-Cat. (B) Quantification of avidin leakage from HUVEC monolayer cultured on different substrates coated with (a) Xlinked PorGel, (b) PorGel, and (c) cfGel-TU-Cat,  $n = 3$ .

characterizing the barrier integrity. According to a previously reported permeability imaging assay, the avidin-biotin system was used to quantitatively assess the integrity of endothelial monolayers.<sup>40</sup> With this assay, increased permeability should allow more avidin to cross the barrier and bind to biotin, indicating compromised cell-cell junctions. First, cells were expanded in PorGel-coated flasks and subsequently seeded onto substrates with different polymer coatings. The formation of HUVEC monolayers was visualized by VE-cadherin (red) staining on all three substrates (Fig. 5A). Leakage of avidin (green) was quantified (Fig. 5B) as described in Experimental section 2.2.12. While HUVEC monolayers on PorGel-coated substrates (b) showed the lowest leakage, no significant increase in leakage was found with monolayers on cfGel-TU-Cat substrates (c). The significantly higher leakage from Xlinked PorGel (a) could be caused by residual GTA. However, it is noteworthy that all the detected leakages are within the range of what is reported for stable and mature HUVEC monolayers, thereby indicating the good quality of the formed endothelial monolayers.<sup>40</sup> Additional experiments with HUVECs expanded in cfGel-TU-Cat-coated flasks also showed the formation of low-leakage monolayers on different substrates (Fig. S5), thus confirming the potential of cfGel-TU-Cat for endothelial cell culture.

### 3.5 Cell signaling

Cell substrates, depending on their chemical composition and mechanical properties, can activate different cell signaling pathways through integrin engagement.<sup>48</sup> To investigate whether culturing the cells on cfGel-TU-Cat alters the activation of cell signaling, the activation of AKT and ERK1/2 (P42/44) were checked.<sup>40</sup> AKT and ERK1/2 are part of the PI3K/AKT and the MAPK/ERK-pathway, respectively. These two pathways regulate cell survival and proliferation of endothelial cells depending on the level of confluency of the cells. The HUVECs were tested on PorGel and cfGel-TU-Cat substrates under both confluent and sparse culture

conditions. As we were specifically interested in the sole influence of the respective biopolymers on cell signaling, we excluded Xlinked PorGel to avoid the presence of any crosslinking agents. As shown in Fig. 6, no significant differences were observed from the phosphorylation of AKT or ERK1/2, thus indicating that cfGel-TU-Cat could be an alternative polymer coating for endothelial cell culture.

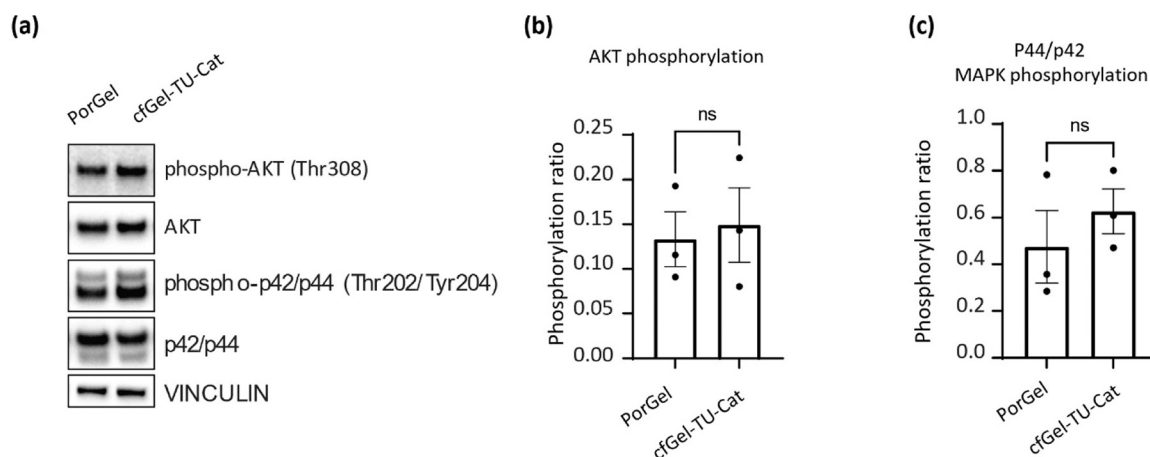
## 4. Conclusion and outlook

In summary, we have synthesized cfGel-TU-Cat as a bio-inspired functional polymer from cold-water fish gelatin with substrate-adhesive properties due to modification with catechol moieties. To explore the potential of this polymer in endothelial cell cultures, we evaluated the substrate-adhesive properties by QCM-D and revealed a greater deposition of cfGel-TU-Cat onto SiO<sub>2</sub> sensors compared to unmodified cfGel, thus confirming the effectiveness of the modifications in promoting substrate-adhesion without the need for additional crosslinking. Substrates coated with cfGel-TU-Cat supported both the adhesion and proliferation of HUVECs to a degree comparable to contemporary porcine gelatin-based coatings and allowed for the formation of confluent endothelial monolayers. Phosphorylation data for both AKT and ERK1/2 further suggests no apparent detrimental effects of cfGel-TU-Cat on cell-signaling pathways. Given the inherent advantages of cold-water fish gelatin over its mammalian counterparts (*e.g.*, low immunogenicity and risk of disease transmission), in addition to the substrate-adhesive properties mediated *via* catechol modification, as well as its suitability as a culture material for HUVECs our study highlights a number of beneficial properties of cfGel-TU-Cat regarding future cardiovascular applications. While the present study serves as an initial evaluation of cfGel-TU-Cat as a coating agent for cardiovascular devices in terms of substrate-binding capabilities and cytocompatible material properties, further studies will be required to solidify its future potential, which will encompass testing of the





## A Confluent culture



## B Sparse culture

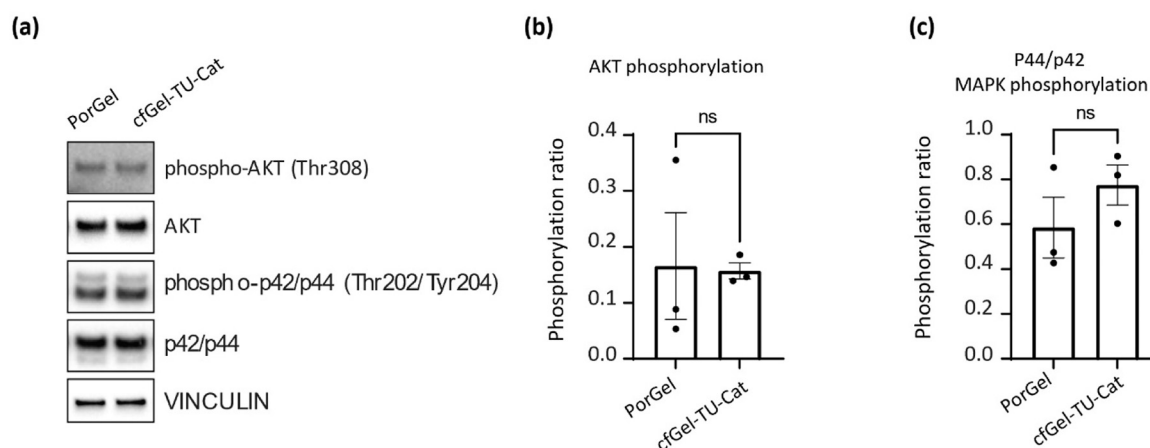


**Fig. 6** Intracellular signaling of HUVECs grown on different substrates. (A) Western blot (a) and relative quantification of AKT (b) and p44/p42 MAPK (c) pathways in confluent culture. (B) Western blot (a) and relative quantification of AKT (b) and p44/p42 MAPK (c) pathways in sparse conditions.

polymer's ability to adhere onto a broader catalogue of substrate materials, including those commonly used to manufacture the targeted cardiovascular devices, as well as the coating-efficiency of the actual devices themselves. Furthermore, *in vivo* studies will be required to evaluate long-term stability of coatings and successful integration of implanted devices.

## Author contributions

T. H.: data curation, formal analysis, investigation, methodology, visualization, writing original draft, writing review and editing. A. A.: data curation, formal analysis, investigation, methodology, visualization, writing original draft, writing review and editing. A. S.: data curation, formal analysis, investigation, methodology, writing original draft, writing review and editing. N. N.: formal analysis, resources, validation, visualization, writing review and editing. W. W.: data curation, formal analysis, investigation, methodology,

writing original draft, writing review and editing. R. M. R.: funding acquisition, resources, supervision, validation, project administration, writing review and editing. C. G.: conceptualization, formal analysis, investigation, resources, validation, visualization, project administration, supervision, writing original draft, writing review and editing. K. W.: conceptualization, formal analysis, investigation, resources, validation, visualization, project administration, supervision, writing original draft, writing review and editing. All authors have given approval to the final version of the manuscript.

## Conflicts of interest

The authors declare no competing financial interest.

## Data availability

The data supporting this article have been included as part of the supplementary information (SI), including antibodies



and reagents; supplementary data Fig. S1–S6 (PDF), including QCM-D measurements of polymer adhesion on glass substrates (Fig. S1), observations of the thermal gelation behavior of porcine gelatin, cfGel, and cfGel-TU-Cat (Fig. S2), an overview of the cell experiments (Fig. S3), cell adhesion and proliferation assay of HUVECs (expanded on cfGel-TU-Cat coated dishes) tested on glass substrates with different surface coatings (Fig. S4), effects of different substrate coatings on monolayer permeability (Fig. S5), and uncropped Western blot data (Fig. S6).

Supplementary information is available. See DOI: <https://doi.org/10.1039/d5lf00218d>.

## Acknowledgements

This work was supported by Empa's Directorate Board (SKINTEGRITY.CH collaborative research program). The authors thank Dr. Janos Vörös from (Department of Information Technology and Electrical Engineering, ETH Zürich) for technical and instrument support for the QCM-D experiment.

## References

- 1 A. Timmis, V. Abovans, P. Vardas, N. Townsend, A. Torbica, M. Kavousi, G. Boriani, R. Huculeci, D. Kazakiewicz, D. Scherr, E. Karagiannidis, M. Cvijic, A. Kaplon-Cieslicka, B. Ignatiuk, P. Raatikainen, D. De Smedt, A. Wood, D. Dudek, E. Van Belle, F. Weidinger and E. S. C. N. C. Societies, *Eur. Heart J.*, 2024, **45**, 4019–4062.
- 2 S. Jana, *Acta Biomater.*, 2019, **99**, 53–71.
- 3 V. W. van Hinsbergh, *Semin. Immunopathol.*, 2012, **34**, 93–106.
- 4 C. T. Esmon, *Chest*, 2003, **124**, 26S–32S.
- 5 J. S. Pober and W. C. Sessa, *Nat. Rev. Immunol.*, 2007, **7**, 803–815.
- 6 C. Wang, L. Cen, S. Yin, Q. Liu, W. Liu, Y. Cao and L. Cui, *Biomaterials*, 2010, **31**, 621–630.
- 7 Q. Cai, W. Liao, F. Xue, X. Wang, W. Zhou, Y. Li and W. Zeng, *Bioact. Mater.*, 2021, **6**, 2557–2568.
- 8 S. E. Motta, P. Zaytseva, E. S. Fioretta, V. Lintas, C. Breymann, S. P. Hoerstrup and M. Y. Emmert, *Front. Bioeng. Biotechnol.*, 2022, **10**, 867877.
- 9 S. Cho, D. E. Discher, K. W. Leong, G. Vunjak-Novakovic and J. C. Wu, *Nat. Methods*, 2022, **19**, 1064–1071.
- 10 D. M. Ibrahim, A. Fomina, C. V. C. Bouten and A. Smits, *Adv. Drug Delivery Rev.*, 2023, **201**, 115085.
- 11 F. Robotti, D. Franco, L. Banninger, J. Wyler, C. T. Starck, V. Falk, D. Poulikakos and A. Ferrari, *Biomaterials*, 2014, **35**, 8479–8486.
- 12 Y. Ding, M. Yang, Z. Yang, R. Luo, X. Lu, N. Huang, P. Huang and Y. Leng, *Acta Biomater.*, 2015, **15**, 150–163.
- 13 A. S. Mertgen, V. T. Trossmann, A. G. Guex, K. Maniura, T. Scheibel and M. Rottmar, *ACS Appl. Mater. Interfaces*, 2020, **12**, 21342–21367.
- 14 C. H. Luu, N. T. Nguyen and H. T. Ta, *Adv. Healthcare Mater.*, 2024, **13**, e2301039.
- 15 R. Schieber, F. Lasserre, M. Hans, M. Fernandez-Yague, M. Diaz-Ricart, G. Escolar, M. P. Ginebra, F. Mucklich and M. Peguerols, *Adv. Healthcare Mater.*, 2017, **6**, 1700327.
- 16 J. Zhao and Y. K. Feng, *Adv. Healthcare Mater.*, 2020, **9**, 2000920.
- 17 A. Gorji, P. J. Y. Toh, H. T. Ong, Y. C. Toh, Y. Toyama and P. Kanchanawong, *ACS Biomater. Sci. Eng.*, 2021, **7**, 2661–2675.
- 18 F. Kuwabara, Y. Narita, A. Yamawaki-Ogata, K. Kanie, R. Kato, M. Satake, H. Kaneko, H. Oshima, A. Usui and Y. Ueda, *Ann. Thorac. Surg.*, 2012, **93**, 156–163.
- 19 J. Zhao, L. Bai, X. K. Ren, J. Guo, S. Xia, W. Zhang and Y. Feng, *Acta Biomater.*, 2019, **97**, 344–359.
- 20 L. Bai, J. Zhao, Q. Li, J. Guo, X. Ren, S. Xia, W. Zhang and Y. Feng, *Macromol. Biosci.*, 2019, **19**, e1800386.
- 21 A. Mahara, T. Sakuma, N. Mihashi, T. Moritan and T. Yamaoka, *Colloids Surf., B*, 2019, **181**, 806–813.
- 22 A. de Mel, G. Jell, M. M. Stevens and A. M. Seifalian, *Biomacromolecules*, 2008, **9**, 2969–2979.
- 23 E. Helfer, S. Kuntz, D. Dion, F. Heim, Y. Georg, F. Thaveau, A. Lejay and N. Chakfe, *JVS-Vasc. Sci.*, 2022, **3**, 193–204.
- 24 L. Weidenbacher, E. Muller, A. G. Guex, M. Zundel, P. Schweizer, V. Marina, C. Adlhart, L. Vejsadova, R. Pauer, E. Spiecker, K. Maniura-Weber, S. J. Ferguson, R. M. Rossi, M. Rottmar and G. Fortunato, *ACS Appl. Mater. Interfaces*, 2019, **11**, 5740–5751.
- 25 K. Kopec, M. Wojasinski, M. Eichler, H. Genc, R. P. Friedrich, R. Stein, R. Singh, C. Alexiou, H. Hlawaty, T. Ciach and I. Cicha, *Biomater. Adv.*, 2022, **134**, 112544.
- 26 K. Su and C. Wang, *Biotechnol. Lett.*, 2015, **37**, 2139–2145.
- 27 V. G. Muir and J. A. Burdick, *Chem. Rev.*, 2021, **121**, 10908–10949.
- 28 A. O. Elzoghby, W. M. Samy and N. A. Elgindy, *J. Controlled Release*, 2012, **161**, 38–49.
- 29 A. B. Bello, D. Kim, D. Kim, H. Park and S. H. Lee, *Tissue Eng., Part B*, 2020, **26**, 164–180.
- 30 A. A. Karim and R. Bhat, *Food Hydrocolloids*, 2009, **23**, 563–576.
- 31 A. L. Alves, J. Costa-Gouveia, J. Vieira de Castro, C. G. Sotelo, J. A. Vazquez, R. I. Perez-Martin, E. Torrado, N. Neves, R. L. Reis, A. G. Castro and T. H. Silva, *Acta Biomater.*, 2022, **141**, 123–131.
- 32 H. J. Yoon, S. R. Shin, J. M. Cha, S. H. Lee, J. H. Kim, J. T. Do, H. Song and H. Bae, *PLoS One*, 2016, **11**, e0163902.
- 33 T. Hammer, K. Yang, T. Spirig, B. Meier-Schiesser, M. Rottmar, K. Maniura-Weber, R. M. Rossi and K. Wei, *Mater. Today Bio*, 2025, **32**, 101701.
- 34 K. Wei, B. Senturk, M. T. Matter, X. Wu, I. K. Herrmann, M. Rottmar and C. Toncelli, *ACS Appl. Mater. Interfaces*, 2019, **11**, 47707–47719.
- 35 A. Zupa, N. Byres, C. Dal Zovo, C. A. Acevedo, I. Angelopoulos, C. Terraza, N. Nestle, P. N. Abarzua-Illanes, F. Quero, P. Diaz-Calderon, Y. Olguin, T. L. Akentjew, C. A. Wilkens, C. Padilla, F. C. Zacconi, K. Pino-Lagos, J. J. Blaker, M. Khoury, J. Enrione and J. P. Acevedo, *Mater. Sci. Eng., C*, 2019, **102**, 373–390.



- 36 R. Levato, K. S. Lim, W. Li, A. U. Asua, L. B. Pena, M. Wang, M. Falandt, P. N. Bernal, D. Gawlitta, Y. S. Zhang, T. B. F. Woodfield and J. Malda, *Mater. Today Bio*, 2021, **12**, 100162.
- 37 B. D. Vogt, E. K. Lin, W.-I. Wu and C. C. White, *J. Phys. Chem. B*, 2004, **108**, 12685–12690.
- 38 F. Orsenigo, C. Giampietro, A. Ferrari, M. Corada, A. Galaup, S. Sigismund, G. Ristagno, L. Maddaluno, G. Y. Koh, D. Franco, V. Kurtcuoglu, D. Poulikakos, P. Baluk, D. McDonald, M. Grazia Lampugnani and E. Dejana, *Nat. Commun.*, 2012, **3**, 1208.
- 39 M. J. Humphries, in *Extracellular Matrix Protocols. Methods in Molecular Biology*, ed. V. A. Sharona Even-Ram, Humana Press, 2009, vol. 522, pp. 203–210.
- 40 F. M. Pramotton, A. Abukar, C. Hudson, J. Dunbar, A. Potterton, S. Tonnichia, A. Taddei, E. Mazza and C. Giampietro, *Mech. Ageing Dev.*, 2023, **213**, 111836.
- 41 R. J. Mosley, M. V. Talarico and M. E. Byrne, *J. Bioact. Compat. Polym.*, 2021, **36**, 261–275.
- 42 J. Saiz-Poseu, J. Mancebo-Aracil, F. Nador, F. Busque and D. Ruiz-Molina, *Angew. Chem., Int. Ed.*, 2019, **58**, 696–714.
- 43 W. Zhang, R. Wang, Z. Sun, X. Zhu, Q. Zhao, T. Zhang, A. Cholewinski, F. K. Yang, B. Zhao, R. Pinnaratip, P. K. Forooshani and B. P. Lee, *Chem. Soc. Rev.*, 2020, **49**, 433–464.
- 44 Y. J. Xu, K. Wei, P. Zhao, Q. Feng, C. K. Choi and L. Bian, *Biomater. Sci.*, 2016, **4**, 1726–1730.
- 45 J. Yu, W. Wei, E. Danner, R. K. Ashley, J. N. Israelachvili and J. H. Waite, *Nat. Chem. Biol.*, 2011, **7**, 588–590.
- 46 J. T. Wolfe, A. Shradhanjali and B. J. Tefft, *Tissue Eng., Part B*, 2022, **28**, 1067–1092.
- 47 A. Kruger-Genge, S. Hauser, A. T. Neffe, Y. Liu, A. Lendlein, J. Pietzsch and F. Jung, *ACS Biomater. Sci. Eng.*, 2021, **7**, 527–540.
- 48 J. Aman and C. Margadant, *Circ. Res.*, 2023, **132**, 355–378.

